Landslides
DOI 10.1007/s10346-019-01333-1
Received: 18 January 2019
Accepted: 27 November 2019

Shiva P. Pudasaini · Michel Jaboyedoff

A general analytical model for superelevation in landslide

Abstract Superelevation is an often observed phenomenon in landslide and debris flow down a complex three-dimensional topography. The degree of superelevation is controlled by the geometry of the channel, the material involved and also the flow dynamics. Empirical methods are usually applied to estimate superelevation. However, those models are incomplete and lack important aspects of the channel geometry, material properties and flow dynamics, instigating serious errors in estimating flow velocities that could only be controlled empirically by introducing ad hoc correction factors. Here, we present new and complete analytical models for superelevation and superelevation velocities down a general topography providing a fully dynamical method. New models formally include essential forces that play an important role in the flow dynamics, namely gravitational forces, topographic- and hydraulic-pressure gradients and Coulomb friction. We discuss the importance of geometry in inducing superelevation and that one directional channel without twist cannot produce superelevation. With the new models we can, in principle, exactly obtain the flow velocities of deformable landslide, dynamic impact pressures and the explicit description of deposition. We have formally provided two alternative analytical representations for superelevation: geometrical and dynamical definitions of superelevation, which is a new concept. We proved that for superelevation to take place, the transversal velocity must have a gradient across the channel. We have analytically constructed a new non-dimensional superelevation number. Superelevation velocity appears to be a non-linear function of the superelevation number. We can now explicitly quantify the superelevation intensity in landslide motion. It has several implications. We proved that superelevation is higher for fluid-saturated debris flows than for dry granular flows. New superelevation models have been validated against a laboratory granular flow down a multi-dimensionally curved channel, and a natural debris flow event in Chamoson, Valais, Switzerland. Our theoretical superelevation velocities appear to be very close to the velocity measured in laboratory and in the field, which however, are largely overestimated by the empirical models. We further validated the model by constructing an exact analytical solution and by applying it to describe superelevation-induced propagation and deposition of the natural debris flow event. New simulations produced observed propagating fronts.

Keywords Analytical model · Landslide · Debris flow · Superelevation

Introduction

Knowledge of the processes associated with the potential natural hazards and their spatial and temporal extent are required for risk management (Leroi et al. 2005; Fell et al. 2008). The dynamical variables, such as the flow velocity and flow height of a landslide or a debris flow, play a crucial role in hazard mitigation and risk management (Guzzetti 2000; Dai et al. 2002). Usually, post-event field investigations provide estimates of some of the debris flow characteristics such as superelevation. For example, if no extended measurements are available, at least the flow marks on banks after a debris flow event allow for the estimation of flow height and flow velocity (Johnson and Rodine 1984; Prochaska et al. 2008; Scheidl et al. 2014). Due to its dynamic characteristics, flow velocity is perhaps the most important variable for designing mitigation structures (Faug 2015; Kattel et al. 2018), and also for simulating the runout of the flow (Hungr and McDougall 2009; Mergili et al. 2017, 2018). Several empirical (Costa 1984; Rickenmann 1999; Jakob 2005), or physics-based (O'Brien et al. 1993; Medina et al. 2008; Hungr and McDougall 2009; Pastor et al. 2009; Christen et al. 2010; Pudasaini 2012; Bregoli et al. 2018; Pudasaini and Mergili 2019), approaches exist for the estimation or computation of debris flow velocities.

Usually, the centrifugal force associated with the channel geometry and the flow dynamics in curved channels results in higher flow height along the outer flank of the channel compared with the flow height along the inner flank. Similarly, field investigations revealed higher, larger and broader lateral deposits on outer sides of channel bends than on inner sides. The difference between these two flow heights is defined as the superelevation (Johnson and Rodine 1984). Information based on superelevation, typically from deposit, is often applied to back-calculate the velocity of a debris flow event (Mizuyama and Uehara 1981; Bertolo and Wieczorek 2005; Scheidl et al. 2014). Thus, the superelevation-induced tilt can be applied for estimation of design flow rates (Johnson and Rodine 1984), which is needed for the construction of engineering structures in mitigating debris flow hazards.

Most of the superelevation models are based on two fundamentally different principles: free vortex and forced vortex. In the free vortex flow assumption, velocity is inversely proportional to the radius of curvature. The fluid mass rotates due to conservation of angular momentum, and Bernoulli's equation can be applied. In contrast, in the forced vortex flow principle, all fluid particles rotate at the constant angular velocity as if it was a solid body, and thus the tangential velocity is directly proportional to the radius of curvature. It produces a parabolic surface profile, and the total energy per unit weight increases with an increase in radius. Superelevation in mass flows, such as avalanches, landslides and debris flows, are classically exclusively modelled with forced vortex methods (Woodward 1920; Schoklitsch 1937; Woodward and Posey 1941; Chow 1959; Apmann 1973; Johnson and Rodine 1984; McClung 2001; Scheidl et al. 2014). However, superelevation in water flows in bends is largely described with models based on free vortex (Thomson 1876; Cunningham 1937; Chow 1959). Due to the prevailing dynamics of dominating to substantial presence of solid-type materials, and also as suggested by the first principles, our present method further supports and generalizes the line of forced vortex. This also covers

Published online: 01 February 2020

superelevation that has probably been largely used in road and railway transportations (Torbic et al. 2014).

Utilizing the tilting surface due to superelevation as the flow passes a given point of the channel, Johnson and Rodine (1984) derived a simple model equation to estimate the mean velocity of the debris flow. To do so, several assumptions were made: (i) A two-dimensional (planar) setting is considered. (ii) As a result of the radial acceleration of the debris, the surface of the flow tilts toward the centre of curvature of the bend at some angle. (iii) The free surface of the debris flow in the cross-section is perpendicular to the direction of radial acceleration of the debris motion. (iv) The debris material is assumed to be an ideal fluid, so no friction and yield strength are considered. Then, by relating the tilt of the flow surface (or, the deposit) to the planar radius of curvature of the channel bend, a mean velocity could be estimated. Measuring the radius of curvature and the tilt at suitably chosen multiple bends (at least two), a mean velocity of the flow can be approximated. However, these implicit assumptions (i–iv) underline the possible limitations of the derived models.

The vortex or forced vortex method (Apmann 1973; McClung 2001) is the most often used empirical method to estimate superelevation. Based on the laboratory debris flow experiments down a twisted channel, Scheidl et al. (2014) studied the influence of material properties and channel radius on the applicability of the forced vortex equation. As in Johnson and Rodine (1984), this approach is also based on several assumptions: the channel of constant radius and rectangular geometry, essentially one-dimensional flow, uniform velocity across the channel, the radius of curvature should exceed the channel width, and the balance between the hydrostatic force and centrifugal force. This probably demanded for the introduction of ad hoc correction factors in those models that may be deemed to have included those aspects of the complex channel topography, and the flow dynamics, which was not possible to formally contain in the empirical models (Scheidl et al. 2014). Scale effect is always a legitimate concern in laboratory experiments compared with the field events (de Haas et al. 2015). However, here, we do not focus on such effects.

Johnson and Rodine (1984) indicated that the empirical models may introduce serious errors in estimating dynamical quantities such as flow velocity. This is so because the derived solutions are not exact, and thus the degree of approximation of the analysis cannot be determined. Furthermore, these models cannot be applied to real three-dimensional channels with strong curvatures and twists as common features of the natural slopes and gullies. This may result in an unusually high velocity for debris flows, and providing a very unrealistic rate of flow at the time when the pulse of debris propagates through the channel (Johnson and Rodine 1984). Such high velocities could only be controlled empirically by introducing some correction factors (Apmann 1973; McClung 2001; Scheidl et al. 2014). Such limitations have not been removed by any existing models. Virtually, there is no further advancement than these basic concepts in modelling complex superelevation in avalanches and debris flows. However, a full analytical model that includes essential physics and geometry of the mass flow incorporating the important process of superelevation is still lacking. Only such a model could provide the physical basis for real application. We address this issue here by presenting a new and more complete analytical model for superelevation down a general channel. The advantage of the new model is that no such assumptions as in empirical methods are needed, and all the essential forces are formally included through associated momentum balances in the flow directions. For example, the channel geometry can be general with variations in both the downslope and cross-slope directions with curvature and twist. Our approach is fully based on the mechanics and dynamics of the flow down a general topography. The model has been validated against a laboratory granular avalanche (of quartz sand) and a natural debris flow event. For the terminology of avalanche and landslide, we refer to Stethem (2013) and Hungr et al. (2014).

Superelevation in laboratory and field

A laboratory experiment of superelevation

Superelevations are observed in curved channels (Thomson 1876; Cunningham 1937; Johnson and Rodine 1984; Pudasaini et al. 2008; Scheidl et al. 2014). Subcritical flows show only slight superelevations whereas supercritical flows can produce strong superelevations (Chow 1959). Superelevation associated with the mass flow is induced jointly by the topographic curvature and torsion, and the flow velocity, or the centrifugal force of the flow. This has been demonstrated in Fig. 1 by a laboratory experiment. Perhaps the term overbanking is more suitable than superelevation, because the phenomenon is related to the description of overbanking along the outer curve.

A natural example of superelevation

Figure 2 shows an example of superelevation during a torrential mudflow. A huge torrential debris flow swept over Chamoson (VS), Switzerland, causing a lot of material damage and evacuation.[1] The material comes mostly from the erosion of schists of Middle Jurassic ages of the Morcles nappes, which was affected by low metamorphism (Badoux 1971). The matrix is made of silty sands and debris, and of massive pieces of schist. The impressive image of the torrential wave suggests that probably a storm has triggered a huge flow that was fluidized as it entered and impacted the town. The river was elevated (overflowed) out of the bed and the torrential mud reached the village of Grugnay in the town of Chamoson. The mud spilled over the bridge. We can see several interesting, and mechanically and dynamically important aspects in this event. The first bend in the upper right clearly shows the superelevation. The associated centrifugal force throws most of the debris material along the outer bend on the side of the superelevated mass that moved a bit farther and eventually stopped as a huge elongated levee. This also reveals the strength of the centrifugal force. The little material deposited on the other side was mainly due to the impact of the debris at the bridge across the channel. Otherwise, all the overbanking debris material lies on the right and is due to the superelevation. The toe (on the lower right in the direction of the flow) of the debris deposit indicates substantial plastic yield strength. Even in this situation, the power of superelevation is tremendous.

Model development

For the equations considered and developed here, (x, y) forms a curved reference surface, where x is the coordinate along the

[1] https://www.lematin.ch/suisse/suisse-romande/lave-torrentielle-devale-chamoson/story/16161089

Fig. 1 (a) A twisted channel used in experiments (Pudasaini et al. 2008): Upper part is straight and inclined at 45°; the middle part is twisted, and the lower part consists of transition and runout zones merging into the horizontal plane. Both the upper and lower parts are cylindrical with radius of 9.7 cm. Total length of the channel = 600 cm, upper straight part = 85 cm, middle twisted part = 365 cm, lower transition part = 50 cm and horizontal flat part = 100 cm. (b) Granular avalanche (of quartz sand) showing the front of superelevated mass induced by the curvature and torsion of the channel. (c) The main body of superelevated avalanche. The avalanching mass is seen in a relatively grey colour around the main bending, whereas the channel is in light grey. The downward arrows in panels B and C indicate the avalanche positions

downslope direction (talweg or guiding curve) of a mountain valley, while y is the arc length in a cross-sectional plane perpendicular to the talweg, and z is the coordinate perpendicular to the reference topography (Fig. 3). This defines an orthogonal curvilinear coordinate system. The model equations are derived in this general coordinate system. The theory presented by Pudasaini and Hutter (2003), and its extension by Pudasaini et al. (2005) that will be utilized here, is designed to model the flow of debris over channels that explicitly includes the general curvature and torsion effects to the flow dynamics in a systematic manner.

As listed in "Notations," first, we define the variables and parameters involved in the model. Let h be the flow depth distribution; u, v be the slope parallel velocity distributions along the downslope and cross-slope directions; and g_x, g_y, g_z be the gravity components along the slope, cross-slope and slope normal directions, respectively. Note that in the present consideration, g_x, g_y, g_z are complex functions of the topography that intrinsically include curvature and torsion (Pudasaini and Hutter 2003). Similarly, $b = b(x, y)$ is the elevation of the basal topography that includes the effects due to channel geometry. The curvature and torsion or twist (e.g. of the guiding curve, or the talweg), $\kappa = \kappa(x)$ and $\tau = \tau(x)$ can be computed from digital elevation data as functions of the arc length of the guiding curve. In what follows, κ and η are the local curvature of the talweg and the accumulation of the torsion of the talweg from an initial position; $\eta = \cos(\theta + \phi(x) + \phi_o)$, where θ is the azimuthal angle (in the cross-slope direction); ϕ_o is a reference value; and $\phi(x) = -\int_{x_o}^{x} \tau(s)ds$ is the accumulation of the torsion τ along the channel, where s is the length along the channel. Note that torsion exists only in three dimensions, whereas curvature exists both in two and three dimensions. Here, we consider a three-dimensional channel for which both the curvature and twist can coexist. κ has the dimension of $[1/m]$, whereas η, in the present consideration, is a dimensionless number (Pudasaini and Hutter 2003; Pudasaini et al. 2005). Furthermore, K_x, K_y are the earth pressure coefficients in the x- and y-directions, respectively, and δ is the basal friction angle, so $\mu = \tan\delta$ is the friction coefficient. The results presented here are relevant for flow of frictional materials down a general channel involving curvature and twist (torsion) that induce superelevation. However, the underlying models may be extended and applied to more viscous and viscoplastic flows (see, "Scope of the model"). For simplicity, we consider a non-inertial flow. Then, following Pudasaini et al. (2005), the force balances along the x- and y-directions for an avalanching mass take the form:

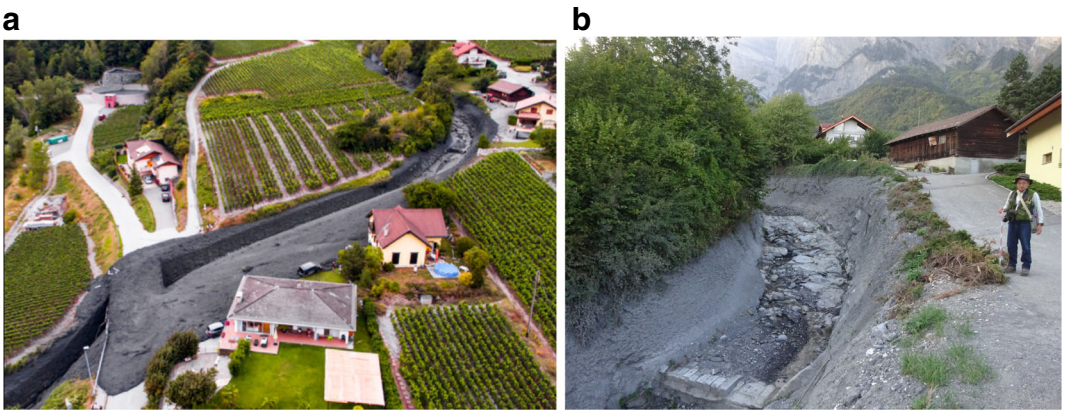

Fig. 2 (a) The mudslide forced the Losentse to come out of bed on Tuesday, August 7, 2018, around 19:15 h CET in Chamoson, Valais, Switzerland. Viewing towards the source. (b) The main bending of the channel after clearing the debris material days after the event

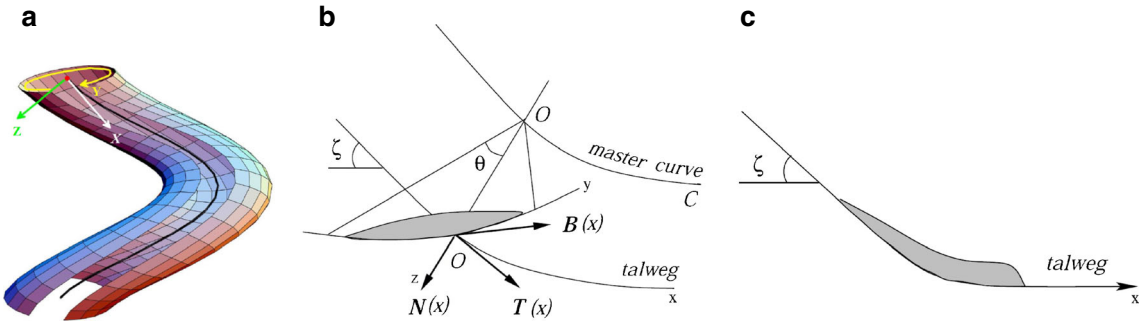

Fig. 3 (a) Representation of a curved and twisted channel, where ***x,y,z*** are the coordinate lines constructed with respect to the master (reference) curve C. The dark line along the channel is the talweg (axis) of the channel. (b) The cross-sectional profile of the landslide with the tangent vectors ***T,N,B*** along the coordinate lines, θ is the azimuthal angle and ζ is the slope along the downhill. (c) The profile of the landslide along the downhill (Pudasaini et al. 2005)

$$h\left[g_x-\frac{u}{|\boldsymbol{u}|}\mu\left(g_z+\kappa\eta u^2\right)-g_z\frac{\partial b}{\partial x}\right]=\frac{\partial}{\partial x}\left[\frac{1}{2}g_zK_xh^2\right], \tag{1}$$

$$h\left[g_y-\frac{v}{|\boldsymbol{u}|}\mu\left(g_z+\kappa\eta u^2\right)-g_z\frac{\partial b}{\partial y}\right]=\frac{\partial}{\partial y}\left[\frac{1}{2}g_zK_yh^2\right], \tag{2}$$

where, $|\boldsymbol{u}|=[u^2+v^2]^{1/2}$ is the magnitude of the total velocity. The first, second and third terms on the left-hand sides of (1) and (2) are forces due to the gravity, Coulomb friction enhanced by extra load induced by curvature and torsion, and the topographic pressure gradients, respectively. The right-hand-side terms are the hydraulic pressure gradients, in the associated flow directions. The later includes lateral pressure enhanced by K_x and K_y. So, the enhanced portion of the effective Coulomb friction force is linearly proportional to κ and η emerging from the geometry of the channel, and quadratically proportional to the velocity u emerging from the flow dynamics, respectively. In $(g_z+\kappa\eta u^2)$, $\kappa\eta u^2$ corresponds to the enhancement in the normal load g_z due to the curvature and twist of the topography. Equations (1) and (2) can be rewritten as:

$$\frac{u}{|\boldsymbol{u}|}\mu\left(g_z+\kappa\eta u^2\right)=g_x-g_z\frac{\partial b}{\partial x}-\frac{1}{h}\frac{\partial}{\partial x}\left[\frac{1}{2}g_zK_xh^2\right]=:F_x, \tag{3}$$

$$\frac{v}{|\boldsymbol{u}|}\mu\left(g_z+\kappa\eta u^2\right)=g_y-g_z\frac{\partial b}{\partial y}-\frac{1}{h}\frac{\partial}{\partial y}\left[\frac{1}{2}g_zK_yh^2\right]=:F_y, \tag{4}$$

where F_x and F_y represent the net driving forces along x- and y-directions, respectively, due to gravity, topographic pressure gradients and the hydraulic pressure gradients. These equations will be utilized to construct a novel superelevation model with superelevation velocities. As explained in "Introduction", often in practice, the information on superelevated height is applied to obtain the flow velocity. So, (1) and (2), or (3) and (4), implicitly assume the flow height h.

Longitudinal velocity

By squaring (3) and (4), and summing them up, we obtain an elegant expression:

$$\mu^2\left(g_z+\kappa\eta u^2\right)^2=F_x^2+F_y^2. \tag{5}$$

The advantage of (5) is that, except the second term on the left-hand side, other terms are independent of u. So, (5) can be solved for u:

$$u=\left[\frac{1}{\mu\kappa\eta}\left\{\left(F_x^2+F_y^2\right)^{1/2}-\mu g_z\right\}\right]^{1/2}, \tag{6}$$

which is the general equation for the longitudinal velocity u with superelevation that is discussed below.

Definition of superelevation

Geometrical definition of superelevation

Classically, superelevation is defined as the positive difference of the elevated heights of the (flowing) mass between the outer curvature (edge or flank) and inner curvature (edge or flank) of the channel (Johnson and Rodine 1984; Allen 1985; de Blasio 2011). In simple words, this is the excess lateral inclination of the flow surface (Pudasaini et al. 2005; Scheidl et al. 2014; von Boetticher et al. 2017). Thus, superelevation, in general, is the transversal gradient of the flow height, i.e. $\partial h/\partial y$, where y measures the transversal (arc) length defining the transversal extent (domain) of the flow. We call this a geometrical definition, or measure, of the superelevation. However, laboratory observation indicates that including other topographic and dynamical effects, the degree or the intensity of superelevation depends on the length of the channel (Pudasaini et al. 2005, 2008).

With the definition of F_y from (4), Eq. (6) can be rewritten in terms of $\partial h/\partial y$ as:

$$\frac{\partial h}{\partial y} = \frac{1}{g_z K_y}\left[g_y - g_z\frac{\partial b}{\partial y} \mp \sqrt{\left(\mu\kappa\eta u^2 + \mu g_z\right)^2 - F_x^2}\right]. \tag{7}$$

As we will see later, (7) provides a general and more complete measure, than those existing, of superelevation. So, (7) is the geometrical representation of superelevation.

Dynamical definition of superelevation

However, as superelevation is the measure of the elevated flow height on one side of the channel compared with the same on the other side, this in fact is induced by the asymmetry of the transversal velocity v. The longitudinal velocity u could be similar across a transversal section, but, for the superelevation to take place, the transversal velocity must have a gradient across the channel. This gradient is mainly induced by the geometry of the channel (thus, gravity and topographic pressure gradients) and the dynamics (hydraulic pressure gradients and the centrifugal force) of the flow itself. In other words, if superelevation takes place, the cross-sectional variation of the transversal velocity provides a measure of superelevation. We call this the dynamical definition, or measure, of superelevation and is formally defined below by (11).

Transversal velocity

With the definition of $|\boldsymbol{u}| = [u^2 + v^2]^{1/2}$, from (4), we have:

$$\frac{v}{[u^2 + v^2]^{1/2}} = \frac{F_y}{\mu\left(g_z + \kappa\eta u^2\right)}. \tag{8}$$

With known u from (6), the transversal velocity v can be extracted from (8). This will be discussed in more detail later.

Superelevation velocity

We call v in (8) the superelevation velocity as this measures the superelevation on one side of the channel slope (the outside bank) compared with the other side. The intensity of superelevation is dynamically determined by the ratio $v/(u^2 + v^2)^{1/2}$, or mechanically by the ratio between the net applied (driving) force and the resisting force, $F_y/\mu(g_z + \kappa\eta u^2)$. This clearly shows that for the flow moving along the talweg (i.e. $v = 0$, for transversally non-deformable material), there is no superelevation. The degree of superelevation is determined by the magnitude of v against the magnitude of the total flow velocity $(u^2 + v^2)^{1/2}$. Note that, even for the downslope motion, v is positive on one side of the mountain flank, while it may become negative on the other side. If v_o and v_i denote the velocities on the outer and the inner flanks of the channel, then, for the superelevation to take place, $|v_o| > |v_i|$ so that the mass elevates higher on the outer flank than on the inner flank.

Superelevation number

We consider (8) and write:

$$\frac{v}{[u^2 + v^2]^{1/2}} = \frac{F_y}{\mu\left(g_z + \kappa\eta u^2\right)} =: \mathcal{S}_N. \tag{9}$$

We call $\mathcal{S}_N$ the superelevation number. Such number does not exist in literature. In gently curved torrent slope and bend, in (4), $(g_y - g_z\partial b/\partial y)$ can be negligible and variations of g_z and K_y with y can be ignored. Then, with the definition of F_y from (4), (9) can be simplified to yield:

$$\mathcal{S}_N = \frac{-g_z K_y(\partial h/\partial y)}{\mu\left(g_z + \kappa\eta u^2\right)}. \tag{10}$$

This is the ratio between the (lateral hydraulic) pressure force and the (Coulomb) friction force. $\mathcal{S}_N$ is high for pressure-dominated flows, but it is low for friction-dominated flows. So, it has important implications. For fluid-saturated debris flows, for which the effective friction is low, $\mathcal{S}_N$ attains high values, resulting in higher superelevation than for dry granular flows. While for friction-dominated flows, i.e. relatively low fluid fraction or dry granular flows, $\mathcal{S}_N$ attains low values, resulting in lower superelevation. Such behaviors are also simulated in Pudasaini et al. (2005) and Pudasaini and Miller (2013).

We note that Shukry (1950) defined $(v^2/(u^2 + v^2)^{1/2}) \times 100$ as strength of a spiral flow (Chow 1959) for water flowing in a curved horizontal channel. However, this definition is ad hoc, whereas we have derived the superelevation number in (9) based on the physical principles, covering both the frictional and viscous or ideal fluids, which can be applied to flows down general channels, and two equivalent dynamical and mechanical expressions for superelevation are presented.

Equation (9) shows that the superelevation number is the ratio between transversal velocity (the superelevation velocity) v and the total flow velocity $(u^2 + v^2)^{1/2}$, or, equivalently, the ratio of net driving force (that includes gravity, topographic pressure gradient and hydraulic pressure gradient) and the resisting force (the Coulomb force). So, from dynamical and mechanical points of view, $\mathcal{S}_N$ is an important non-dimensional number.

Equation (9) leads to the following analytical solution for v:

$$v = \pm\frac{u\mathcal{S}_N}{\left[1 - \mathcal{S}_N^2\right]^{1/2}}. \tag{11}$$

Equation (11) shows that the ratio between the transversal and longitudinal velocities can be rewritten as a function of the superelevation number $\mathcal{S}_N$:

$$\frac{v}{u} = \pm\mathcal{I}(\mathcal{S}_N), \tag{12}$$

where, $\mathcal{I}(\mathcal{S}_N) = \mathcal{S}_N/\left(1 - \mathcal{S}_N^2\right)^{1/2}$ is the superelevation intensity. So, ultimately, the superelevation velocity is a function of the superelevation number $\mathcal{S}_N$. Furthermore, for v to be real, $1 - \mathcal{S}_N^2$ must be

positive. This means, $\mu^2\left(g_z+\kappa\eta u^2\right)^2 > F_y^2$. This is realistic because, in rapid channel flows, usually u is large, and in total, the magnitude of F_y is relatively small. In the limit as $v \to 0$, $\mathcal{S}_N \to 0$; and as $u \to 0$, $\mathcal{S}_N \to 1$, or when lateral forces are negligible, $\mathcal{S}_N \to 0$, and when F_y balances Coulomb friction force, then $\mathcal{S}_N \to 1$. So, the superelevation number $\mathcal{S}_N$ lies in the domain (0, 1). In the limit, when the total transversal driving force is significantly higher than the friction force, then $\mathcal{S}_N \to 1$, and superelevation is very effective. In this situation, the superelevation intensity can be substantially high to very high. But, when the total lateral driving force is significantly lower than the friction force, then $\mathcal{S}_N \to 0$, and the superelevation is negligible. For this, the superelevation intensity can be disregarded. Alternatively, for mainly downhill motion, as $\mathcal{S}_N \to 0$, $\mathcal{I}(\mathcal{S}_N) \to 0$. However, for the high-intensity superelevation, or the lateral expansion fan in the transition and deposition regions, $\mathcal{I}(\mathcal{S}_N)$becomes very large because $\mathcal{S}_N \to 1$. For given material parameters, basal topography and flow height, (6) and (12) constitute the full analytical model for velocities with superelevation.

Figure 4 shows the superelevation intensity (v/u or, $\mathcal{I}(\mathcal{S}_N)$) as a function of superelevation number. With this, we have now the possibility to explicitly quantify the superelevation in landslide motion. The superelevation intensity as shown in Fig. 4 is within the range of observed data in the laboratory and in the field (Scheidl et al. 2014). This justifies the usefulness of the new superelevation model. Furthermore, we mention that superelevation may not arise at all even in a curved channel (Chow 1959). We have proven this, and this has been demonstrated in Fig. 4 by showing that this happens if the superelevation intensity approaches zero. This is so because the force that tends to produce the superelevation (e.g. the centrifugal force) can be balanced by the complex forces, for example due to the lateral gravity force and the lateral topographic pressure gradients that are included in F_y.

It is interesting to observe that from (3) and (4), we can directly obtain:

$$\frac{v}{u} = \frac{F_y}{F_x}. \tag{13}$$

However, in contrast to (12), (13) does not directly involve the normal load, or the frictional contribution $\mu(g_z + \kappa\eta u^2)$. The advantage is that it is valid for any ratio of F_y and F_x. However, as discussed earlier, the friction force leads to a constraint on $\mathcal{S}_N$ such that $\mathcal{S}_N$ must lie in the domain (0, 1), usually as $F_y < F_x$, $v < u$. Nevertheless, in the transition and deposition regions, or in regions of substantially large superelevation, $F_y > F_x$, and thus $v > u$. This also applies to strongly curved channels for which u drops rapidly to zero, but at the same time, due to the lateral spreading, v is relatively much higher than u. In situations when $v \gg u$, superelevation is amplified and thus, $\mathcal{S}_N \to 1$. Furthermore, (13) indicates that the superelevation, or the transversal velocity, is directly proportional to F_y and the longitudinal velocity u. F_y is positive on the one side of the channel, and negative on the other side; they, in general, have different magnitudes and higher positive value than the negative value. This difference is caused by the different effective gravity, normal load and hydraulic pressure gradients (Apmann 1973; Johnson and Rodine 1984; McClung 2001; Pudasaini et al. 2005; Pudasaini et al. 2008). Thus, whether or not the superelevation takes place will be determined by the difference in the magnitude of F_y on either side (flank) of the channel.

Alternative geometrical definition of superelevation

Here, we provide an alternative geometrical definition of superelevation. Applying the definition of F_y, we can solve (8) for $\partial h/\partial y$ to yield:

$$\frac{\partial h}{\partial y} = \frac{1}{g_z K_y}\left[g_y - g_z\frac{\partial b}{\partial y} - \mu\left(g_z+\kappa\eta u^2\right)\frac{v}{\left(u^2+v^2\right)^{1/2}}\right]. \tag{14}$$

Instead of F_x in (7), (14) includes more dynamical aspect as represented by the factor $v/(u^2+v^2)^{1/2}$. In a gently curved channel, (14) may reduce to:

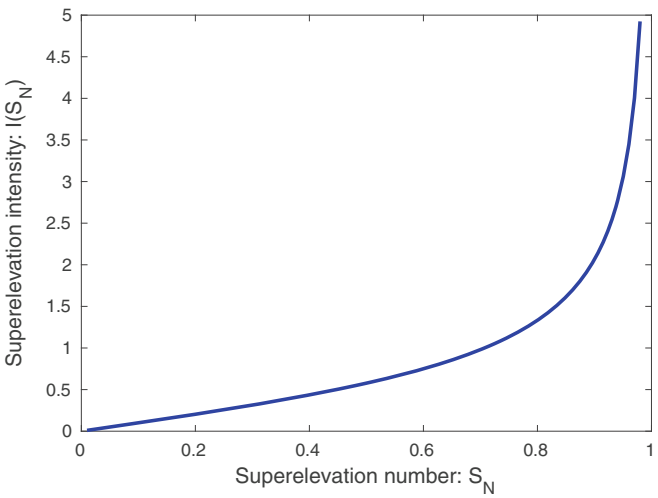

Fig. 4 Superelevation intensity as a function of the superelevation number

$$\frac{\partial h}{\partial y} = -\frac{\mu}{g_z K_y}\left(g_z + \kappa\eta u^2\right)\frac{v}{(u^2+v^2)^{1/2}}. \tag{15}$$

This proves that the superelevation is proportional to the lateral flow velocity, and the magnitude is amplified by the ratio between the lateral velocity and the total velocity.

With (15), we further consider different scenarios. Usually, during the rapid down slope motion, $u > v$, then:

$$\frac{\partial h}{\partial y} = -\frac{\mu}{g_z K_y}\left(g_z + \kappa\eta u^2\right)\frac{v}{u}. \tag{16}$$

In the depositional region, slowly, v may overtake u, so:

$$\frac{\partial h}{\partial y} = -\frac{\mu}{g_z K_y}\left(g_z + \kappa\eta u^2\right). \tag{17}$$

Before this, momentarily, both velocity components may be comparable, then:

$$\frac{\partial h}{\partial y} = -\frac{\mu}{g_z K_y}\left(g_z + \kappa\eta u^2\right)\frac{1}{\sqrt{2}}. \tag{18}$$

However, if the lateral velocity is negligible, for example for laterally negligible or no deformation, (15) leads to:

$$\frac{\partial h}{\partial y} = 0. \tag{19}$$

So, for different flow dynamical situations, we can explicitly quantify the associated superelevations. This importantly contributes in design of channels and banks in bendings. Further, a crucial fact (19) formally proves is that, for superelevation to exist, the lateral velocity must be non-zero. Such a formal proof is novel. We also mention that even the most simplified form (17) represents more information on superelevation than the classical superelevation models (Woodward 1920; Schoklitsch 1937; Woodward and Posey 1941; Chow 1959; Apmann 1973; Johnson and Rodine 1984; McClung 2001; Scheidl et al. 2014). This will be further elaborated later.

Scope of the model

Although the model equations developed above are primarily based on the frictional rheology, it can be extended and applied to more viscous-type flows, or the flows with higher water contents and pore water pressures. This can be achieved by extending the friction coefficient μ to the effective friction coefficient $\mu_e = (1-\lambda)\mu$, where λ is the pore pressure ratio (Iverson and Denlinger 2001). The factor $(1-\lambda)$ will also affect gravity components, and hydraulic and basal pressure gradients. This has been explained in Pudasaini et al. (2005). With this enhancement, the new model can then be applied to highly fluidized mass flows, also for volcanic and submarine events (Pudasaini and Miller 2013). Moreover, cohesion can be included in Coulomb friction term that extends μg_z, and also the earth pressure coefficients K_x, K_y. Furthermore, the model can also be extended to real two- or multi-phase mixture flows (Pudasaini 2012; Pudasaini and Mergili 2019).

The torrential debris and mud flows are often viscous flows. As in Pudasaini et al. (2005), Pudasaini (2012) and Pudasaini and Mergili (2019), viscous effects could also be added explicitly on the right-hand sides of (1) and (2). However, this adds complexity that may hinder the direct and explicit solution of the velocity fields from these equations. Yet, the viscoplastic rheology can be modelled either by using a complex effective Coulomb-type mixture friction coefficient that includes both the viscous and plastic properties of the bulk (Pokhrel et al. 2018; Khattri and Pudasaini 2018, 2019), or directly a viscoplastic approach might be adopted (Domnik et al. 2013; von Boetticher et al. 2016). However, the latter approach could be much more complex.

Discussions on important aspects of the new model

Here, we point out some important features of the new model equations: (6) and (12).

Importance of different forces in superelevation and flow stopping

The new models (6) and (12) include different forces that play an important role in the flow dynamics resulting in superelevation, namely gravity, topographic pressure gradients and hydraulic pressure gradients in both the downslope and cross-slope directions, and the Coulomb friction force. We focus on the downslope flow velocity u given by (6), which is enhanced by the dynamic forces F_x and F_y, and reduced by the frictional force $-\mu g_z$. The magnitude of u is controlled by the unified parameter $P_u = \mu\kappa\eta$ that includes the basal friction coefficient μ, and the curvature κ and twist η of the slope. Note that μ and η in this representation are dimensionless parameters, and κ has the dimension of $[1/m]$ which is also the dimension of P_u. The parameter P_u can be determined from the knowledge of the slope (e.g. through GIS) and the flow material. This will be discussed later. Here, deposition refers to the halting or stoppage of the mass flow, i.e. $u \to 0$. The flow tends to stop (in the longitudinal direction) if one of the following four conditions are met.

I. μ very large: This corresponds to the very large basal friction, which effectively halts the flow of the material, a type of fully sticky bottom, or full interlocking of the flow material with the basal surface. However, note that μ might vary locally (Jop et al. 2006; Pudasaini and Hutter 2007; Mergili et al. 2018). So, higher values of u are associated with lower values of μ.
II. κ very large: This means the radius of curvature ($R = 1/\kappa$) is very small. Since the flowing mass experiences a very large curvature as it enters the region of strongly curved topography, the mass tends to stop or deposit. As normal load is proportional to κ, a very large κ enhances the normal load in the similar manner. The basal shear stress increases accordingly, resulting in the halting of the flowing mass. This is evident in Fig. 2.
III. η very large: As for κ, a strongly twisted channel tends to force the flowing mass to stop. However, note that κ and η are independent geometric parameters, both influencing the flow dynamics (Pudasaini et al. 2005).

IV. $\left(F_x^2+F_y^2\right)^{1/2}-\mu g_z \approx 0$: This means that when the total net driving force is balanced by the frictional force, the mass flow stops, which means mass deposits.

I–III are related to the material and topographical properties of the slope, whereas IV is associated with the net force $\left(\left(F_x^2+F_y^2\right)^{1/2}\right)$ that enhances the motion and the resisting force $(-\mu g_z)$ that opposes the motion. Whereas u is inversely proportional to μ, κ and η, or the unified parameter $P_u=\mu\kappa\eta$, u is directly proportional to $\left(F_x^2+F_y^2\right)^{1/2}-\mu g_z$. So, I–III and IV influence u fundamentally differently.

An explicit description of deposition

Dynamically, a complete deposition of mass in both directions is attained when both the longitudinal and transversal velocities vanish, i.e. $|u|=0$ and $|v|=0$. First, we analyse u. As discussed above, (6) tells us that $u\to 0$ if $P_u\to\infty$, or $\left(F_x^2+F_y^2\right)^{1/2}-\mu g_z\to 0$. This means that the total enhancing force $\left(F_x^2+F_y^2\right)^{1/2}$ must be balanced by friction $-\mu g_z$. So, $\left(F_x^2+F_y^2\right)^{1/2}-\mu g_z\le 0$, i.e. friction must overcome the driving force. Now, we analyse the transversal velocity. Equation (12) says that $v\to 0$ if $u\to 0$ or, $\mathcal{S}_N\to 0$. However, $u/\left(1-\mathcal{S}_N^2\right)^{1/2}=u/\left[1-F_y^2/\mu^2\left(g_z+\kappa\eta u^2\right)^2\right]^{1/2}$ can be of the order unity even if $u\to 0$. For example, assume u is very small, then $u^2\ll u$, so, $u/\left(1-F_y^2/\mu^2 g_z^2\right)^{1/2}\to O(1)$. Thus, effectively $v\to 0$ if $\mathcal{S}_N\to 0$, i.e. $F_y/\mu(g_z+\kappa\eta u^2)\to 0$, which means that either one of μ, κ or η is very large, or $F_y\to 0$. Hence, the mass flow comes to a halt if $P_u\to\infty$, or $(\left(F_x^2+F_y^2\right)^{1/2}-\mu g_z\le 0$, and $F_y\to 0)$.

If the lateral velocity $v\to 0$, then $F_y\to 0$. So, if the longitudinal velocity vanishes (e.g. in the runout), then $F_y=\mu g_z$, i.e. the lateral forces are balanced by friction, also leading to the halting of the flow in the lateral direction.

Alternatively, from the total velocity, $\boldsymbol{u}=(u,v)$, we obtain its magnitude as:

$$|\boldsymbol{u}|=\left[\frac{1}{\mu\kappa\eta}\left\{\left(F_x^2+F_y^2\right)^{1/2}-\mu g_z\right\}\right]^{1/2}\frac{\left[\mu^2\left(g_z+\kappa\eta u^2\right)^2-F_y^2\right]^{1/2}}{\mu\left(g_z+\kappa\eta u^2\right)}. \tag{20}$$

So, $u\to 0$ and $\mu^2 g_z^2-F_y^2\to 0$ are conditions for the total stop of the mass, i.e. $|\boldsymbol{u}|\to 0$.

Longitudinal motion caused by lateral forces

A plausible and counterintuitive observation is the effect of the transversal net driving force F_y and the twist η of the topography on enhancing or reducing u. Usually, one would think that the longitudinal velocity u can be obtained by considering the net downslope force F_x, curvature κ and the resisting force $-\mu g_z$. However, we have formally proved that this is not true. In fact, u also depends on the net transversal force F_y and the twist η. This can also be explained physically. For example, consider a situation when the mass enters the runout zone, which is flat along x, but channel opens into a fan in the y, or transversal, direction. This is often the situation in the fan region. Locally, we may assume that the hydraulic pressure gradient in the x-direction is almost zero, which is a reasonable approximation for a longitudinally long fan with plateau-type deposition. Then, F_x is almost zero. However, (6) shows that F_y can be substantially large that contributes positively to u. The question may arise for why the lateral pressure may cause or enhance longitudinal motion. This can be explained and justified physically. For a deformable mass flow, the motion in one direction is also influenced by the topographic changes and hydraulic pressure gradients in that and the other direction. Interestingly, v explicitly depends only on F_y and u, but u depends on F_x and F_y. So, ultimately, v also depends both (directly) on F_y, and (indirectly) on F_x. For example, at a strongly curved channel such as the right bend, $u\to 0$ but v can be very large.

Estimating velocities and pressures

Measuring, or inferring, the flow depth is relatively (much) easier than the flow velocities. The model equations, (6) and (12), indicate that with the knowledge of the topography, friction and the flow depth, in principle, we can fully obtain the flow velocities in both the longitudinal and transversal directions. From an application point of view, even more important is the determination of the (dynamic) impact pressures in flow directions, $p_x=C_x\rho u^2$, and $p_y=C_y\rho v^2$, for some suitable coefficients C_x and C_y, typically 1/2, where ρ is the material density, and u and v are given by (6) and (12). The total or the resultant impact pressure can be obtained as $p_t=C_x\rho u^2+C_y\rho v^2$, or $p_t=C_t\rho(u^2+v^2)$ (for a suitable choice of C_t, see, e.g. Kattel et al. (2018)). Such description of flow dynamics via u, v, and the estimation of impact pressures, that include gravitational forces, topographic pressure gradients, hydraulic pressure gradients, friction coefficient, curvature and twist, is new.

Comparison with existing models

The analytical models presented in (6) and (12) are general. In order to compare these models with the existing models, assume uniform flow in x-direction (i.e. $\partial h/\partial x=0$) and the flow takes place on the reference surface. Then, following the designated coordinate lines, from (6) we obtain:

$$u=\left[\frac{1}{\mu\kappa\eta}\left\{\left(g_x^2+\left(g_y-g_z K_y\frac{\partial h}{\partial y}\right)^2\right)^{1/2}-\mu g_z\right\}\right]^{1/2}. \tag{21}$$

Furthermore, if the gravity forces in x- and y-directions are assumed negligible (e.g. as in transition and deposition zones in runout fans), then $F_x=0$. If one could think of neglecting the lateral gravity component and the Coulomb friction, then, with $g_z=g\cos\zeta$, where ζ is the slope angle, and $R=1/\kappa$ is the radius of curvature, (6) reduces to:

$$u=\left[R\left(\frac{1}{\mu\eta}\right)(g\cos\zeta)\frac{\partial}{\partial y}\left(K_y h\right)\right]^{1/2}. \tag{22}$$

Equation (22) can be written in discrete form. With the channel width (or arc) $B=\Delta y$, associated with the superelevation $\Delta h=K_{y_p}h_o-K_{y_a}h_i$, where h_o and h_i are the flow heights in the outer and inner curvatures of the channel, and K_{y_p} and K_{y_a} are

associated with the outer and the inner parts of the flow assuming that the flow is compressed and expanded in these local regions (McClung 2001; Scheidl et al. 2014), (22) reduces to:

$$u = \left[R\left(\frac{1}{\mu\eta}\right)(g\cos\zeta)\frac{\Delta h}{B}\right]^{1/2}. \tag{23}$$

This corresponds to the superelevation model by Scheidl et al. (2014). An equation similar to (23) has also been obtained by Johnson and Rodine (1984). Nevertheless, in both Johnson and Rodine (1984) and Scheidl et al. (2014), friction and twist do not appear (i.e. equivalently $\mu = 1$, and $\eta = 1$), and $\Delta h/B$ = tangent of the tilt of the free surface. However, their simplified approach does not include any dynamics of superelevation, e.g. $\partial(K_y h)/\partial y$, that automatically appears in our model (6). Their approach only accounts for the highest markings on the channel sides that might have been produced by two different surges of substantially different dynamics. This can result in potentially large errors.

If, moreover, the hydraulic pressure gradient is assumed to be a constant, $\partial h/\partial y = H$, and $K_y = 1$, $\mu = 1$, $\eta = 1$, then, per unit channel width, (22) further reduces to:

$$u = [g\cos\zeta HR]^{1/2}, \tag{24}$$

Equation (24), in the form, is similar to the model presented by De Blasio (2011), but here it is without the assumption of equality of curvatures on either flanks of the slope.

However, from the physical point of view, the validity of (23) and (24) that are obtained from (6) after imposing several simplifying assumptions mentioned above can be questioned (Johnson and Rodine 1984). In fact, (23) and (24) may not represent the true physics of the velocity corresponding to the superelevation of mass flow in a multi-dimensionally curved channel. This is clear from the derivation of (6). All, or most of the assumptions made above in obtaining the reduced forms (23) and (24), tend to distort the physics of superelevation. For example, experiments show, for the superelevation to take place, the channel must be curved in both x- and y-directions, and that the curvature κ and twist η must be present (Pudasaini et al. 2008; Scheidl et al. 2014). In fact, superelevation is the result of the twist of the topography that corresponds to $\eta \neq 1$ (Pudasaini and Hutter 2003; Pudasaini et al. 2005). Furthermore, gravity and friction are other important aspects of the mass flow that plays a crucial role in determining u. Thus, (23) and (24) lack the physical ground to represent the velocity of a mass flow associated with the superelevation, whereas (6) or (7) provides the full and general analytical description of mass flow down a general channel with superelevation.

The previous approaches of modelling superelevation are largely based on ad hoc and empirical methods. Our analysis shows that the previous models are imperfect and only consider very few aspects of superelevation while we have presented a more general, complete and mechanics-based approach for superelevation. In our approach, no correction factor is needed to be introduced, in contrast to those in the vortex-based models (Scheidl et al. 2014). The ad hoc or empirically introduced correction factors which reflect the uncertainties of those approaches (as high as a factor of 10) likely stem from the fact that the previous approaches were incomplete, and very weakly associated with the physics of the process. Our model replaces the empirical factor by the mechanically and automatically emerging factor $1/P_u = 1/\mu\kappa\eta$, and the inclusion of gravity force g_x and the friction force $-\mu g_z$. Scheidl et al. (2014) found that the channel slope as well as centreline radius has a significant influence on the superelevation through the correction factor used in the vortex equation. This indicates that the three-dimensional topographic effects that are present in our derivation of (6) cannot be neglected, which was ignored in the derivation of the reduced models (23) and (24) to compare the previous models (de Blasio 2011; Scheidl et al. 2014). The value of the unified parameter P_u can be geometrically and mechanically estimated, making our model physically based. This is explained in "Importance of different forces in superelevation and flow stopping".

Importance of geometry in inducing superelevation

A crucial aspect in inducing superelevation is the direct influence of the topography on the gravity force components g_x, g_y and g_z by the curvature, and mainly by the twist, of the basal surface. Superelevation cannot be generated in a channel that is curved only in one direction. Twist is the essential mechanism in generating the superelevation (Pudasaini et al. 2005, 2008; Scheidl et al. 2014). So, the reduced models in (23) and (24) (Apmann 1973; Johnson and Rodine 1984; McClung 2001; de Blasio 2011; Scheidl et al. 2014) cannot fully describe the superelevation because it only includes curvature in the x-direction which can only reduce the speed of mass flow in the x-direction depending on the curvature intensity. Only the twist can elevate the flowing mass more on the outer than the inner bank of the channel. So, in general, a one-directional channel without twist cannot produce superelevation. Furthermore, the topographic pressure gradients play a crucial role in inducing the superelevation (Pudasaini et al. 2005, 2008). Equations (23) and (24), which neglect $\partial b/\partial x$ and $\partial b/\partial y$, and the twist, cannot legitimately generate superelevation.

Superelevation in transportation lines

Probably, the design of railway lines and roads finds the most prominent use of the concept of superelevation by design practitioners (Torbic et al. 2014). This is so because as a vehicle moves around a curve it experiences a centripetal acceleration and the friction at the interface between the tire (wheel) and road is counterbalanced by the superelevation.

Now we show how (21) can be utilized to better design the superelevation in road, highway and railway lines. For simplicity and compatibility to most road and rail lines, by assuming a gentle downslope, (21) can be rewritten as:

$$g\cos\zeta K_y\frac{\partial h}{\partial y} = \mu\left(g\cos\zeta + \frac{\eta}{R}u^2\right), \tag{25}$$

or,

$$\frac{\partial h}{\partial y} = \left(\frac{\mu\eta}{K_y\cos\zeta}\right)\frac{u^2}{gR} + \frac{\mu}{K_y}. \tag{26}$$

In the form, (26) can be compared to the superelevation model suggested by the National Cooperative Highway Research

Program, Transportation Research Board, USA (Torbic et al. 2014). In their notations:

$$\frac{e}{100} = \frac{u^2}{gR} - f, \tag{27}$$

where, $e/100$ corresponds to the superelevation ($\partial h/\partial y$) and f corresponds to friction (μ) in (26). In mildly twisted pavements, η can be set to unity, and for a point vehicle K_y is also unity. However, there are still fundamental differences between these two models.

(i) The sign of the second term on the right-hand sides of (26) and (27) is of major concern, so is the first term. Our model (26) is based on the principle of Coulomb friction that is very well known to enhance the normal load $g\cos\zeta$ by the centrifugal force $\eta u^2/R$ due to the presence of curvature ($\kappa = 1/R$) at the bend (Savage and Hutter 1991; Tai et al. 2002; Pudasaini and Hutter 2007; Fischer et al. 2012). So, the first term on the right-hand side of (26), that is due to the centrifugal force, and the second term therein, that is due to the normal load, must have the same sign. In the model (27), the superelevation is given just by the centrifugal force minus the friction. However, in contrast to (27), in our model (26), the frictional part appears with the same sign as the centrifugal force. This is due to the fact that the Coulomb frictional force is proportional to the total dynamical load ($g\cos\zeta + \eta u^2/R$) enhanced by the centrifugal force, rather than just to the static load $g\cos\zeta$ without the centrifugal contribution.

(ii) The second important aspect is the factor $\mu\eta/K_y\cos\zeta$ in (26) that does not appear in (27). This means that our model extends the superelevation of a point mass travelling on a horizontal plain curve (Torbic et al. 2014) to deformable mass down a more general channel (Pudasaini et al. 2005). This is so, because in our model, variables, such as $\partial h/\partial y$ and u, depend on the position at the channel. Normally, the factor $\mu\eta/K_y\cos\zeta$ is less than unity. This means the centrifugal force is reduced by this factor in our model. However, this reduction is consistently covered by the term μ/K_y, as this is a positive quantity. In general, quantitatively, (26) and (27) can produce quite different results.

(iii) The negative sign in the second term on the right-hand side of (27) is due to the choice of the direction of the friction force along the lateral direction. However, by definition, the frictional force must act against the direction of the driving gravitational force direction. So, in the derivation of (26), the direction of friction is considered along the component of the lateral gravitational force.

There are major differences in the two modelling approaches. Our method is fully supported by the principle of the Coulomb friction. And, our model covers much wider physics of mass flow, even for a point mass travelling along horizontal bends. So, this analysis demonstrates that we have presented a fundamentally advanced and physically consistent model for superelevation.

Model applications

Pudasaini et al. (2005, 2008) presented detailed simulations showing the effect of the torsion on the dynamics and depositions of debris and avalanche flows, and the validation of the full model by laboratory experiments. Here, we focus on the application of the new superelevation models developed in this contribution. We consider two situations: a laboratory granular flow (Fig. 1), and a natural debris flow event (Fig. 2). However, the new model should further be scrutinized by extensively testing it with different laboratory experiments (e.g. including Scheidl et al. 2014) and the field events (e.g. 2018 Chamoson event, VS, Switzerland).

Laboratory avalanche experiment

First, consider the granular flow experiments down a curved and twisted channel (Pudasaini et al. 2008). We validate our superelevation velocity (21) along the downslope. As the front of avalanche reaches the transition zone, the front velocity in the experiment in Fig. 1 was about $u = 2.25$ ms^{-1}. We note that due to the torsion, all the x, y and z directional gravity components are evolving as a function of the torsion. Since the torsion induces the twist in the channel, the effective normal load increases substantially as the flow moves downslope. Following the experimental setup and the material parameters, we obtained estimations on the parameters and dynamical variables. We compare the experimental velocity and the velocity from the new model around the transition in the lower portion of the channel. For detailed information, we refer to Pudasaini et al. (2008). For the present consideration, at this transition, due to channel curvature, the normal load g_z is typically enhanced by a factor of 1.3. This is reasonable and justified because based on the complexity of the channel, g_z is implicitly enhanced by the curvature and twist of the channel (Pudasaini and Hutter 2003; Pudasaini et al. 2005). The bed friction coefficient was $\mu = 0.47(1 - \gamma h)$, where, following Pudasaini and Hutter (2007), friction is assumed to decrease with the pressure (normal load) that is modelled with the pressure parameter $\gamma = 0.16$ (also, see, Potyondy 1961), the channel slope was $\zeta = 45^\circ$ and the mean slope in the transversal direction, $\zeta_l \approx 30^\circ$. Other estimated quantities are $\eta = 0.8$, $\kappa = 2.0$, $\partial h/\partial y = 0.8$. Furthermore, since the pressure is in the passive state, and the flow is still rapid, it is legitimate to consider $K_y = 1.2$ that includes a mild passive pressure coefficient (Pudasaini and Hutter 2007). With this, from (21) we obtain $u \approx 2.27$ ms^{-1}, which is very close to the velocity estimated from the experiment, $u = 2.25$ ms^{-1}. However, if we apply the reduced model (23), we obtain $u \approx 3.4$ ms^{-1} which is much higher than the experimental velocity. To bring it down to the observed value, we need to apply the correction factor $K = 2.3$, which is a typical correction factor used in literature dealing with empirical models (Hungr et al. 1984; Chen 1987; Bulmer et al. 2002; Scheidl et al. 2014).

This analysis shows that the ad hoc velocity correction factors in the previous empirical models are introduced to substantially control the unrealistically high velocities. This was due to the fact that those models could not include the important energy dissipation mechanisms such as friction, twist and passive earth pressure due to compaction in the outer curvature region and deposition.

[2] https://www.youtube.com/watch?v=aGNISaAjbxU

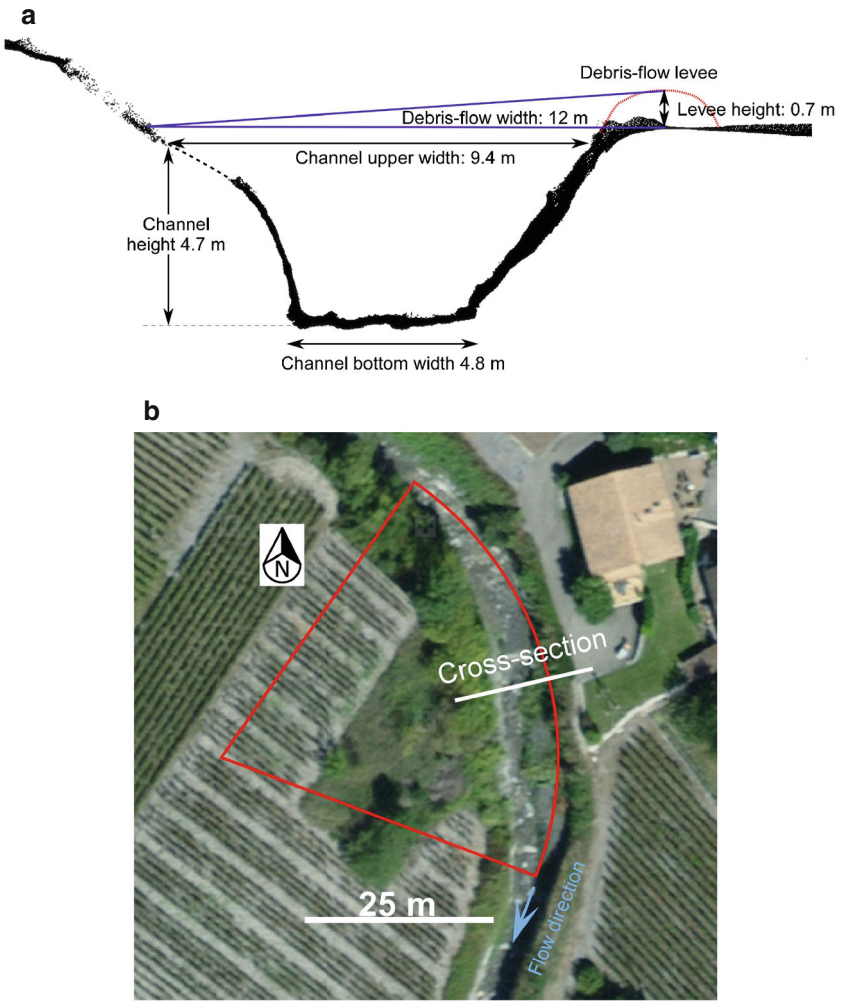

Fig. 5 Field data of the Chamoson debris flow event by lidar: flow extent and channel (a), and bending or transversal section (b), with radius of curvature (image from Swisstopo). The slope is 12%, the radius 44 m and the angle of the curved flow path is 76°

Debris flow in Chamoson

Estimation of the superelevation velocity

The channel cross section was obtained using a Structure from Motion (SfM) model combined with a handheld lidar. We used a Phantom 4 drone to recreate the topography (SfM) and the GeoSlam (handheld lidar) for the channel. SfM was obtained by using PhotoScan software (Agisoft 2015), and lidar was acquired with a handheld ZEB REVO from GeoSlam. The front of the debris flow has been visually tracked from the timed video footage.[2] In combination with the detailed textured topography in point cloud format, it was possible to translate those timed observations on the 3D terrain model. This allowed us to obtain both the time and position differences, which gave us the flow velocity. Visualisation of the 3D model has been greatly facilitated by the use of the CloudCompare open-source software (Girardeau-Montaut 2006). The estimated flow front velocity of the Chamoson event is about $u = 6$ ms^{-1}. As in the laboratory granular flow, we also calculated the superelevation velocity for the Chamoson event from our new model. The physical and geometrical parameters obtained from the field visit (Fig. 5) are as follows: $\zeta = 12^{\circ}$, $\mu = 0.47(1 - \gamma h)$, $\gamma = 0.16$, $\kappa = 1/44$. As explained above, this also assumes that the basal friction decreases with normal load as modelled by the parameter γ. The effective maximum change in the flow height from bottom to the top is about $\Delta h = 4.7 + 0.7 = 5.4$ m. The laterally curved hydraulic perimeter, including extension beyond the peak is $2 \times 4.7 + 4.8 + 2.6 + 1.7 = 18.5$ m $= \Delta y$. This provides $\partial h/\partial y$, with respect to the laterally curved coordinates. The lateral slope (corresponding to g_y) is determined by joining the central point of the channel to the distal end of the flow at the outer margin, which is about $2.4 + 2.6 + 1.7 = 6.7$ m. This, with the effective elevation change of 5.0 m, provides the mean lateral slope of about $\zeta_l = 36°$. To include the bend-induced compaction and twist, we used moderate values of $K_y = 1.1$ and $\eta = 0.9$. However, these are some plausible estimations of the geotechnical (K_y) and geometrical (bending or twist η) parameters. Although these parameters are physically based, the choice of their numerical values should be further explored with sensitivity analysis (Mergili et al. 2017; Mergili et al. 2018), which, however, is

not within the scope here. Similarly, the curvature and twist significantly enhance the normal load, which here is modelled by enhancing the normal load g_z by about 30% which is reasonable for such a strongly curved channel. Such enhancement of g_z has been justified at "Laboratory avalanche experiment". With this, applying the superelevation velocity (21), we obtain $u \approx 6.6$ ms^{-1}. This value is close to the one estimated from the event, including field visit and video. However, the reduced model (23) results in $u \approx 8$ ms^{-1} which is much higher than the reality. This shows similar discrepancy as in the granular flow experiments discussed above, requiring a correction factor 2. However, the error in measurement can be comparable to the reduced uncertainty of the model.

Superelevation induced propagation and deposition

With the above legitimate estimations of the superelevation velocities, both for the laboratory and field events, next, we further explore the possibility to apply our model to qualitatively describe the superelevation-induced propagation and deposition of the debris flow in Chamoson (Fig. 2). However, here, we do not aim to perform direct and full dynamical simulation of the event. Consider the mass balance equation along the channel (Pudasaini et al. 2005):

$$\frac{\partial h}{\partial t} + \frac{\partial (hu)}{\partial x} = 0. \tag{28}$$

For the flow along the channel close to the deposition, such as the one in Chamoson, the cross-slope contributions might be neglected, and η can be set equal to unity because the torsion is weak, but the curvature is strong. So, (6) reduces to:

$$u = \left[\frac{1}{\mu\kappa}\left\{g_x - g_z\left(K_x\frac{\partial h}{\partial x} + \mu\right)\right\}\right]^{1/2}. \tag{29}$$

This can be written as:

$$u = \alpha\sqrt{1-\beta\frac{\partial h}{\partial x}}, \tag{30}$$

where, $\alpha = \sqrt{(g_x - \mu g_z)/\mu\kappa}$, and $\beta = K_x g_z/(g_x - \mu g_z)$. Then, from (28) and (30), we obtain:

$$\frac{\partial h}{\partial t} + \frac{\partial}{\partial x}\left(\alpha h\sqrt{1-\beta\frac{\partial h}{\partial x}}\right) = 0. \tag{31}$$

This leads to a complex, non-linear advection and diffusion equation for the kinematic wave:

$$\frac{\partial h}{\partial t} + C\frac{\partial h}{\partial x} - D\frac{\partial^2 h}{\partial x^2} = 0, \tag{32}$$

where the advection and diffusion coefficients C and D are complex and non-linear functions of the material and geometrical parameters, and evolving flow depth h, and the hydraulic pressure gradient $\partial h/\partial x$: $C = C(\alpha, \beta; \partial h/\partial x) = \alpha\sqrt{1-\beta(\partial h/\partial x)}$, and $D = D(\alpha, \beta; h, \partial h/\partial x) = \alpha\beta h/2\sqrt{1-\beta(\partial h/\partial x)} = \alpha^2\beta h/2C$. So, $\alpha = C$ corresponds to a typical wave speed when $\partial h/\partial x$ vanishes, i.e. the tip of the front head, top of the forehead or stretched main body or the tail part of the flow where the pressure gradients could be negligible. In this situation, the diffusion coefficient reduces to $D = \alpha\beta h/2 = K_x g_z h/2\sqrt{\mu\kappa(g_x - \mu g_z)}$. This shows that the diffusion varies with the flow depth. Further interesting aspects are the following: Low friction (μ) implies high advection and diffusion. Similarly, the flow advection and spreading (reduction in flow height) are reduced around high bendings, which means flow moves slowly and flow depth increases around bendings. Both of these dynamic responses are physically justified. This discussion also implies that not the α and β, but C and D are physically more relevant. Since α and β are positive quantities, C is higher in the front than in the main body. So, the advective flux in the front is higher than in the main body and the tail. However, due to the structure of D, the diffusive flux behaves inversely to the advective flux. These characteristics determine the form of the deforming debris mass.

Depositional behaviour

The near deposit flow behaviour can be described by the steady-state flow condition for which (31) reduces to a non-linear ordinary differential equation:

$$\frac{dh}{dx} = \mathcal{A} - \frac{\mathcal{B}}{h^2}, \tag{33}$$

where both $\mathcal{A} = (g_x - \mu g_z)/g_z K_x$, and $\mathcal{B} = \mu\kappa\, \mathcal{C}_0/g_z K_x$ are functions of physical and geometrical parameters, and $\mathcal{C}_0$ is a constant of integration. Here, $\mathcal{B}$ appears to be a linear function of the channel curvature. This equation can be solved exactly and analytically to obtain:

$$x = \frac{h}{\mathcal{A}} - \frac{1}{\sqrt{\mathcal{A}/\mathcal{B}}\,\mathcal{A}}\tanh^{-1}\left[\sqrt{\mathcal{A}/\mathcal{B}}\,h\right] + \mathcal{C}, \tag{34}$$

where $\mathcal{C}$ is a constant of integration that can be fixed by the boundary condition for the flow height at a given location.

Figure 6 shows the solution of the mass distribution that is similar to the Chamoson debris flow event as described by the simple analytical model (34), for $\mathcal{A} = 1$, $\mathcal{B} = 1, 3, 5$ (low, medium and high curvatures) and $\mathcal{C} = 1.9$. The solution captures well the depositional characteristics, the mass (geometry) distribution and the blunt toe of the front head. Another important feature of the new solution is that as the curvature increases, the lateral flow depth along the channel bank increases. This is in line with the mechanics of the curvature-induced superelevation because higher curvature means higher superelevation that results in higher depositional depth.

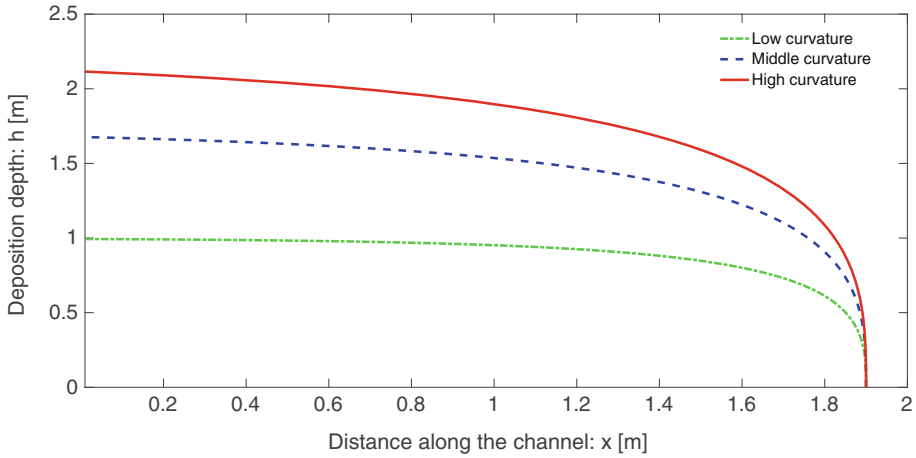

Fig. 6 Analytical solution for the superelevation-induced deposition of the Chamoson debris flow event as modelled by (34)

Propagating front

Equation (32) is a challenge to solve analytically; however, we solved it numerically by applying the high-resolution TVD-NOC methods (Tai et al. 2002; Pudasaini 2011). Basal friction is a critical parameter in mass flows. As explained earlier in the sections "Importance of different forces in superelevation and flow stopping" and "An explicit description of deposition", it decreases with the pressure, and thus the flow depth. Following Pudasaini and Hutter (2007), we may assume that μ decreases with the flow depth: $\mu = \mu_0(1 - \gamma h)$, where $\gamma = 0.5$ is a typical value, and $\mu = \mu_0$ is the pressure independent static friction coefficient. The values of $\alpha = 6.0$ and $\beta = 1.0$ are used for simulation. α can be adjusted with scaled time. The corresponding time evolution of the debris flow front is shown in Fig. 7. Qualitatively, this is in line with the propagating front of the Chamoson debris flow event.

Summary

Superelevation is observed in mass flows taking place in curved channels that is induced jointly by the topographic curvature and torsion, and the flow velocity, or the centrifugal force of the flow, as common features of natural slopes and gullies. Empirical methods, such as forced vortex, are often used to estimate superelevation. However, these methods are based on ad hoc correction factors as they lack the important aspects of the complex channel topography and the flow dynamics. Those models could not be appropriately applied to real three-dimensional channels with strong curvature and twists. So, empirical models may introduce serious errors and result in unusually high velocities and flow rates. Such high velocities could only be controlled empirically by introducing some correction factors. As those models are not exact, the degree of approximation of the analysis could not be determined. Such limitations have not yet been removed by any existing models.

We have addressed these issues by presenting a new, complete model for superelevation down a general topography providing a fully dynamical method. Following the first principle and the mechanics and dynamics of flow, we have derived general analytical models for superelevation and superelevation velocities. New models do not require those assumptions as in empirical methods. They formally include essential forces that

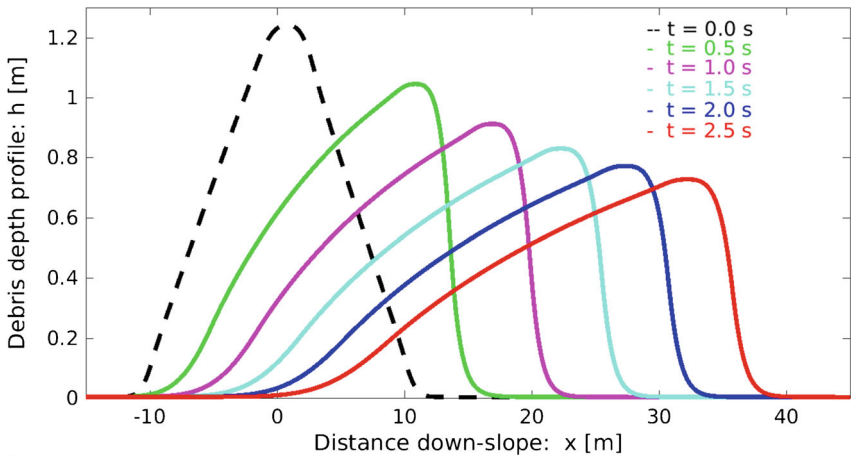

Fig. 7 Propagating front of the debris flow as modelled by (32)

play important role in the flow dynamics, namely gravitational forces, topographic pressure gradients, hydraulic pressure gradients and the Coulomb friction force (so, the basal friction, curvature and twist of the slope). With the new analytical models, in principle, we can exactly obtain the flow velocities, and (dynamic) impact pressures. So, such descriptions are fundamentally new. We have formally provided alternative analytical definitions for superelevation: (i) The geometrical definition of superelevation. This is defined as the positive difference of the elevated flow heights between the outer curvature and inner curvature of the channel. (ii) Dynamical definition of superelevation: This is a fully new concept which relates the superelevation to the asymmetry of the transversal velocity. So, for the superelevation to take place, the transversal velocity must have a gradient across the channel. Whether or not the superelevation takes place is determined by the difference in the magnitude of the effective longitudinal force on either side of the channel. We have also presented analytical descriptions for the halting of the flow associated with the material and topographical properties of the slope and the net force.

As an important non-dimensional number, we have analytically constructed a new superelevation number. It is the ratio between the transversal velocity to the total flow velocity, or, equivalently, the ratio of net driving force and the resisting frictional force. It has several important implications. The intensity and degree of superelevation are determined dynamically or mechanically. We proved that superelevation is higher for fluid-saturated debris flows than for dry granular flows. We further revealed that the superelevation velocity is a function of the superelevation number. We have now the possibility to explicitly quantify the superelevation intensity in landslide motion.

New models are reduced after imposing several simplifying assumptions to compare with the existing empirical models. However, the reduced models turned out to be unrealistic, and do not represent the true physics of the velocity corresponding to the superelevation in a multi-dimensionally curved channel. This is so because, for the superelevation to take place, the channel must be curved in both flow directions, and that the curvature and twist must be present. Furthermore, gravity and friction play a crucial role in determining the superelevation. A fundamentally important aspect in inducing superelevation is the direct influence of the topography on the gravity force components, by the curvature and twist of the basal surface. Similarly, the topographic pressure gradients play an important role in inducing superelevation. Classical models lack these aspects. In contrast to the vortex-based models, our approach does not require the empirically introduced correction factors, which stems from the fact that those approaches were incomplete and are weakly associated with the physics of the process. Our analysis shows that empirical models only consider some aspects of superelevation while we have presented a more general, complete and mechanics-based approach for superelevation.

Some aspects of the new superelevation model have been validated. We have applied the model against a laboratory granular flow down a curved and twisted channel, and a natural debris flow event. Our theoretical superelevation velocity appears to be very close to experimental velocity, which however, is largely overestimated by the empirical model without a correction factor. We further validated our model by applying it to describe superelevation-induced propagation and deposition of the 2018 Chamoson debris flow event in Switzerland. For this, we constructed an analytical solution for the depositional geometry, which qualitatively captured well the observed characteristics. Furthermore, we developed a new, complex, non-linear advection and diffusion equation for the kinematic wave. The simulation of this model produces propagating front similar to that observed in the Chamoson debris flow event.

Acknowledgements

We thank the reviewers, editor and the editorial board for their constructive comments and suggestions that largely improved the quality and clarity of the paper. We are grateful to Jose Pularello and Jeremie Voumard for their support to acquire and interpret the lidar and SfM data, for photogrammetric work and creation of Fig. 5. Shiva P. Pudasaini gratefully thanks the Herbette Foundation for providing financial support for Sabbatical visit to the University of Lausanne, Switzerland for the year 2018, April–June, where this contribution was triggered.

Funding information

This work has been financially supported by the German Research Foundation (DFG) through the research project PU 386/5-1: "A novel and unified solution to multi-phase mass flows: $U^{MultiSol}$".

Notations

b	basal surface of flow
B	channel width
$\mathcal{A}, \mathcal{B}$	functions of physical, geometrical parameters
C	master curve
C, D	non-linear advection, diffusion coefficients
C_x, C_y, C_t	coefficients of (dynamic) impact pressures, total pressure
$\mathcal{C}, C_0$	constant of integration
e	corresponds to superelevation in transportation lines
f	corresponds to friction in transportation lines
F_x, F_y	net driving forces along x, y
g	gravity constant
g_x, g_y, g_z	components of gravitational acceleration
H	assumed hydraulic pressure gradient
h	debris flow depth
h_o, h_i	flow depths in outer and inner curvatures of channel
$\mathcal{I}$	$=\mathcal{I}(\mathcal{S}_N)$, superelevation intensity
K	empirical superelevation correction factor
K_x, K_y	earth pressure coefficients
K_{y_p}, K_{y_a}	passive/active K_y on outer/inner flanks
O	coordinate origin, at master curve or talweg
p_x, p_y, p_t	(dynamic) impact pressures, total pressure
P_u	$=\mu\kappa\eta$, unified parameter
R	$=1/\kappa$, radius of curvature
s	length along the channel
$\mathcal{S}_N$	superelevation number
t	time
u, v	velocity components along x, y

$\boldsymbol{u}$	$=(u, v)$
v_o, v_i,	velocities on outer and inner flanks of slope
x, y, z	coordinate lines/flow directions
α, β	advection, diffusion flux parameters
γ	pressure parameter
δ	basal friction angle
ζ, ζ_l	channel slope angle, mean lateral slope
η, ϕ,	ccumulation of torsion
θ	azimuthal angle
κ	curvature
λ	pore pressure ratio
μ; μ_e, μ_o	$=\tan\delta$, friction coefficient; static, effective μ
τ	torsion
ϕ_o	reference value of ϕ

References

Agisoft LLC (2015) Agisoft PhotoScan user manual, professional edition, version 1.2.6

Allen JRL (1985) Principles of physical sedimentology. Springer, New York

Apmann RP (1973) Estimating discharge from superelevation in bends. J Hydraul Div, ASCE 99:65–79

Badoux H (1971) Feuille 1305 Dt de Morcles et notice explicative Atlas geol. Suisse 1:25000. Comm. geol. Suisse

Bertolo P, Wieczorek GF (2005) Calibration of numerical models for small debris flows in Yosemite Valley, California, USA. Nat Hazards Earth Syst Sci 5:993–1001

Bregoli F, Medina V, Bateman A (2018) TXT-tool 3.034-2.1 a debris flow regional fast hazard assessment toolbox, in: Landslide dynamics: ISDR-ICL landslide interactive teaching tools. https://doi.org/10.1007/978-3-319-57777-7_10

Bulmer MH, Barnouin-Jha OS, Peitersen MN, Bourke M (2002) An empirical approach to studying debris flows: implications for planetary modeling studies. J Geophys Res 107:9–1–9-14. https://doi.org/10.1029/2001JE001531

Chen CL (1987) Comprehensive review of debris flow modelling concepts in Japan. Geol Soc Am Rev Eng Geol 7:13–29. https://doi.org/10.1130/REG7-p13

Chow VT (1959) Open channel hydraulics. McGrayv-Hill Book Company, New York

Christen M, Kowalski J, Bartelt P (2010) RAMMS: numerical simulation of dense snow avalanches in three-dimensional terrain. Cold Reg Sci Technol 63:1–14

Costa JE (1984) Physical geomorphology of debris flows. In: Costa JE, Fleisher P (eds) Developments and applications of geomorphology. Springer-Verlag, Berlin, pp 268–317

Cunningham B (1937) River flow around bends. Nature 140:728–729

Dai FC, Lee CF, Ngai YY (2002) Landslide risk assessment and management: an overview. Eng Geol 64(1):65–87. https://doi.org/10.1016/S0013-7952(01)00093-X

de Blasio FV (2011) Introduction to the physics of landslides: lecture notes on the dynamics of mass wasting. Springer, Berlin

de Haas T, Braat L, Leuven JRFW, Lokhorst IR, Kleinhans MG (2015) Effects of debris flow composition on runout, depositional mechanisms, and deposit morphology in laboratory experiments. J Geophys Res Earth Surf 120:1949–1972

Domnik B, Pudasaini SP, Katzenbach R, Miller SA (2013) Coupling of full two-dimensional and depth-averaged models for granular flows. J Non-Newton Fluid Mech 201:56–68

Faug T (2015) Depth-averaged analytic solutions for free-surface granular flows impacting rigid walls down inclines. Phys Rev E:92. https://doi.org/10.1103/PhysRevE.92.062310

Fell R, Corominas J, Bonnard C, Cascini L, Leroi E, Savage WZ (2008) Guidelines for landslide susceptibility, hazard and risk zoning for land use planning. Eng Geol 102(3):85–98. https://doi.org/10.1016/j.enggeo.2008.03.022

Fischer JT, Kowalski K, Pudasaini SP (2012) Topographic curvature effects in applied avalanche modeling. Cold Reg Sci Technol 74:21–30

Girardeau-Montaut, D (2006) Detection de changement sur des donnees geometriques tridimensionnelles. PhD Thesis, Telecom ParisTech. https://tel.archives-ouvertes.fr/pastel-00001745/

Guzzetti F (2000) Landslide fatalities and the evaluation of landslide risk in Italy. Eng Geol 58:89–107

Hungr O, McDougall S (2009) Two numerical models for landslide dynamic analysis. Comput Geosci 35:978–992

Hungr O, Morgan GC, Kellerhals R (1984) Quantitative analysis of debris torrent hazards for design of remedial measures. Can Geotech J 21(4):663–677. https://doi.org/10.1139/t84-073

Hungr O, Leroueil S, Picarelli L (2014) The Varnes classification of landslide types, an update. Landslides 11(2):167–194

Iverson RM, Denlinger RP (2001) Flow of variably fluidized granular masses across three-dimensional terrain: 1. Coulomb mixture theory. J Geophys Res 106(B1):537–552

Jakob M (2005) Debris-flow hazard analysis. In: Jakob and Hungr (eds) Debris-flow hazards and related phenomena, pp 411–443

Johnson AM, Rodine JR (1984) Debris flow. In: Brunsden D, Prior DB (eds) Slope instability, pp 257–361

Jop P, Forterre Y, Pouliquen O (2006) A constitutive law for dense granular flows. Nature 441:727–730

Kattel P, Kafle J, Fischer JT, Mergili M, Tuladhar BM, Pudasaini SP (2018) Interaction of two-phase debris flow with obstacles. Eng Geol 242:197–217

Khattri KB, Pudasaini SP (2018) An extended quasi two-phase mass flow model. Int J Non Linear Mech 106:205–222

Khattri KB, Pudasaini SP (2019) Channel flow simulation of a mixture with a full-dimensional generalized quasi two-phase model. Math Comput Simul 165:280–305

Leroi E, Bonnard Ch, Fell R, McInnes R (2005) "Risk assessment and management. In: Hungr O., Fell R., Couture R. (Eds.) Landslide risk management, Vancouver, Proceedings of International Conference on Landslide Risk Management, Vancouver, Canada,31 May-02 June, 139–198

McClung DM (2001) Superelevation of flowing avalanches around curved channel bends. J Geophys Res 106:16489–16498

Medina V, Hürlimann M, Bateman A (2008) Application of FLATModel, a 2D finite volume code, to debris flows in the northeastern part of the Iberian Peninsula. Landslides 5:127–142

Mergili M, Fischer JT, Krenn J, Pudasaini SP (2017) r.avaflow v1, an advanced open-source computational framework for the propagation and interaction of two-phase mass flow. Geosci Model Dev 10:553–569. https://doi.org/10.5194/gmd-10-553-2017

Mergili M, Emmer A, Juricova A, Cochachin A, Fischer JT, Huggel C, Pudasaini SP (2018) How well can we simulate complex hydro-geomorphic process chains? The 2012 multi-lake outburst flood in the Santa Cruz Valley (Cordillera Blanca, Peru). Earth Surf Process Landf 43:1373–1389

Mizuyama T, Uehara S (1981) Debris flow in steep slope channel curves. Jpn J Civ Eng 23:243–248

O'Brien JS, Julien PY, Fullerton WT (1993) Two dimensional water flood and mudflow simulation. J Hydraul Eng ASCE 119:244–261

Pastor M, Haddad B, Sorbino G, Cuomo S, Drempetic V (2009) A depth-integrated, coupled SPH model for flow-like landslides and related phenomena. Int J Numer Anal Methods Geomech 33:143–172

Pokhrel PR, Khattri KB, Tuladhar BM, Pudasaini SP (2018) A generalized quasi two-phase bulk mixture model for mass flow. Int J Non Linear Mech 99:229–239

Potyondy PG (1961) Skin friction between various soils and construction materials. Geotechnique 11:339–353

Prochaska AB, Santi PM, Higgins JD, Cannon SH (2008) A study of methods to estimate debris flow velocity. Landslides 5:431–444

Pudasaini SP (2011) Some exact solutions for debris and avalanche flows. Phys Fluids 23(4):043301. https://doi.org/10.1063/1.3570532

Pudasaini SP (2012) A general two-phase debris flow model. J Geophys Res 117:F03010. https://doi.org/10.1029/2011JF002186

Pudasaini SP, Hutter K (2003) Rapid shear flows of dry granular masses down curved and twisted channels. J Fluid Mech 495:193–208

Pudasaini SP, Hutter K (2007) Avalanche dynamics: dynamics of rapid flows of dense granular avalanches. Springer, Berlin

Pudasaini SP, Mergili M (2019) A multi-phase mass flow model. J Geophys Res Earth Surf. https://doi.org/10.1029/2019JF005204

Pudasaini SP, Miller SA (2013) The hypermobility of huge landslides and avalanches. Eng Geol 157:124–132

Pudasaini SP, Wang Y, Hutter K (2005) Modelling debris flows down general channels. Nat Hazards Earth Syst Sci 5:799–819

Pudasaini SP, Wang Y, Sheng LT, Hsiau SS, Hutter K, Katzenbach R (2008) Avalanching granular flows down curved and twisted channels: theoretical and experimental results. Phys Fluids 20:073302. https://doi.org/10.1063/1.2945304

Rickenmann D (1999) Empirical relationships for debris flows. Nat Hazards 19:47–77

Savage SB, Hutter K (1991) The dynamics of avalanches of granular materials from initiation to runout. Part I: analysis. Acta Mech 86:201–223

Scheidl C, McArdell BW, Rickenmann D (2014) Debris-flow velocities and superelevation in a curved laboratory channel. Can Geotech J 52:305–317
Schoklitsch A (1937) "Hydraulic structures" translated from the German by Samuel Shulitz. Am Soc Mech Eng New York I:151
Shukry A (1950) Flow around bends in an open flume. Trans Am Soc Civ Eng 115:751–779
Stethem C (2013) Avalanches. In: Bobrowsky PT (ed) Encyclopedia of natural hazards. Encyclopedia of Earth Sciences Series. Springer, Dordrecht
Tai YC, Noelle S, Gray JMNT, Hutter K (2002) Shock-capturing and front-tracking methods for granular avalanches. J Comput Phys 175:269–301
Thomson J (1876) On the origin and winding of rivers in alluvial plains, with remarks on the flow around bends in pipes. Proc R Soc London 25:5–8
Torbic DJ, O'Laughlin MK, Harwood DW, Bauer KM, Bokenkroger CD, Lucas LM, Ronchetto JR, Brennan S, Donnell E, Brown A, Varunjikar T (2014) Superelevation criteria for sharp horizontal curves on steep grades. National Cooperative Highway Research Program, NCHRP REPORT 774. Transportation Research Board, Washington, D.C.
von Boetticher A, Turowski JM, McArdell BW, Rickenmann D, Kirchner JW (2016) Debrisintermixing-2.3: a finite volume solver for three-dimensional debris-flow simulations with two calibration parameters-part 1: model description. Geosci. Model Dev 9:2909–2923
von Boetticher A, Turowski JM, McArdell BW, Rickenmann D, Hürlimann M, Scheidl C, Kirchner JW (2017) DebrisInterMixing-2.3: a finite volume solver for three-dimensional debris-flow simulations with two calibration parameters - part 2: model validation. Geosci Model Dev 10(706):3963–3978
Woodward SM (1920) Hydraulics of the Miami flood control project. Miami Conservancy District, Technical Report, Pt. VII, Daytron, Ohio
Woodward SM, Posey CJ (1941) Hydraulics of steady flow in open channels. Wiley, New York, p 112

S. P. Pudasaini (✉)
Institute of Geosciences, Geophysics Section,
University of Bonn,
Meckenheimer Allee 176, D-53115, Bonn, Germany
Email: pudasaini@geo.uni-bonn.de

M. Jaboyedoff
Faculte des geosciences et de l'environnement, Risk-group - ISTE - Institute of Earth Sciences,
University of Lausanne,
GEOPOLIS - 3793, CH-1015, Lausanne, Switzerland